Available online at www.sciencedirect.com
ScienceDirect
Remote Sensing of Environment 112 (2008) 2605–2614
Remote Sensing of Environment
www.elsevier.com/locate/rse

Derivation of melt pond coverage on Arctic sea ice using MODIS observations

Mark A. Tschudi [a,*], James A. Maslanik [b,1], Donald K. Perovich [c,2]

[a] Research Affiliate, CCAR, University of Colorado, Boulder, CO 80309, United States
[b] University of Colorado, Aerospace Engineering Sciences Dept., CCAR, UCB431, Boulder, CO 80309, United States
[c] USACE Engineer Research and Development Center, Cold Regions Research and Engineering Laboratory, 72 Lyme Road, Hanover, NH 03755-1290, United States

Received 12 December 2006; received in revised form 17 December 2007; accepted 22 December 2007

Abstract

The formation of meltponds on the surface of sea ice during summer is one of the main factors affecting variability in surface albedo over the ice cover. However, observations of the spatial extent of ponding are rare. To address this, a MODIS surface reflectance product is used to derive the daily melt pond cover over sea ice in the Beaufort/Chukchi Sea region through the summer of 2004. For this region, the estimated pond cover increased rapidly during the first 20 days of melt from 10% to 40%. Fluctuations in pond cover occurred through summer, followed by a more gradual decrease through late August to 10%. The rapid initial increase in pond cover occurred later as latitude increased and melt progressed northward.

A surface campaign at Barrow in June 2004 provided pond and ice spectral reflectance needed by the MODIS algorithm to deduce pond coverage. Although individual pond and ice reflectance varies within the comparatively small region of measurement, the mean values used within the algorithm ensured that relevant values (i.e. concurrent with satellite observations) were being applied.

Aerosonde unpiloted aerial vehicles (UAVs) were deployed in June 2004 from Barrow, Alaska, to photograph the sea ice so melt pond cover could be estimated. Although the agreement between derived pond cover from UAV photos and estimates from MODIS varies, the mean estimates and distribution of pond coverages are similar, suggesting that the MODIS technique is useful for estimating pond coverage throughout the region. It is recommended that this technique be applied to the entire Arctic through the melt season.

Keywords: Sea Ice; Arctic; MODIS; UAV

1. Introduction

Sea ice extent in the Arctic Ocean has been decreasing an estimated 2–4% per decade over the course of the satellite record and has reached minimum coverage in recent years (Comiso, 2002; Serreze et al., 2003; Stroeve et al., 2008). Recent evidence suggests that the ice has also been thinning (Maslanik et al., 2007; Rothrock et al., 2003). The reduction of sea ice extent and thickness is enhanced by the ice-albedo feedback (Curry et al., 1995), accelerating the rate of ice melt in the Arctic summer. Recent field and modeling studies (Perovich et al., 2002a) have determined that to accurately represent the ice-albedo feedback it is necessary to correctly ascertain the timing and duration of the seasonal variations in the surface albedo. The key period is June through July, when the incident solar energy is relatively large and the surface albedo is changing rapidly. The appearance of melt ponds after Arctic summer sea-ice melt onset has a significant impact on the strength of this positive feedback mechanism, by lowering the albedo of the ice pack. Melt ponds appear in depressions on first-year and multiyear ice, and are formed by the runoff produced from melting snow and ice. As melt ponds form and evolve, there are large changes in their spectral signatures at visible and near-infrared wavelengths.

Melt ponds have an enormous impact on lowering the ice cover albedo. The increase in fractional coverage of melt ponds during

* Corresponding author. Tel.: +1 303 565 0774.
E-mail addresses: marktschudi@gmail.com (M.A. Tschudi), james.maslanik@colorado.edu (J.A. Maslanik), donald.k.perovich@erdc.usace.army.mil (D.K. Perovich).
[1] Tel.: +1 303 492 8974.
[2] Tel.: 603 646 4255.

0034-4257/$ - see front matter © 2008 Elsevier Inc. All rights reserved.
doi:10.1016/j.rse.2007.12.009

melt (Perovich et al., 2002b; Tschudi et al., 2001) is the primary factor in the reduction of albedo on summer sea ice. Eicken et al. (2004) found a linear decrease in albedo as a function of pond fraction. Although the albedo of bare, multiyear ice varies little during melt, ponded ice albedo typically decreases during the melt season, as ponds grow deeper and the underlying ice thins.

As summer progressed during the Surface Heat Budget of the Arctic Ocean (SHEBA) experiment, melt pond coverage began to decrease in late July and continued in this fashion until fall freeze-up (Perovich et al., 2002b; Tschudi et al., 2001). This exemplifies the importance of properly quantifying the pond coverage throughout summer, since the appearance and evolution of ponds is a two-stage process, with fractional extent increasing during early summer and decreasing in late summer. Since the onset of melt varies over the Arctic Ocean (Anderson & Drobot, 2001), it follows that pond coverage will evolve differently in separate locations. Thus, to properly ascertain how ponds accelerate the summer melt, there is a need to represent their coverage over an extensive area and throughout the melt season.

Sea ice concentration is typically estimated using satellite-based passive microwave observations. Melt ponds on sea ice result in the underestimation of summertime sea ice concentration in passive microwave frequencies, since melt ponds appear radiometrically similar to open water (Cavalieri et al., 1984; Fetterer & Untersteiner, 1998). Large-scale estimates of melt pond coverage would thus lead to improvements in ice concentration for assimilation into sea ice models, as well as real-time ice coverage forecasting.

Arctic melt pond coverage has been measured in several Arctic locations during separate field experiments (Eicken et al., 1994; Maykut et al., 1992; Perovich & Tucker, 1997; Tucker et al., 1999) and has been observed aerially (El Naggar et al., 1998; Perovich et al., 2002b; Tschudi et al., 1997, 2001; Yackel et al., 2000) and with high-resolution satellite imagery (Fetterer & Untersteiner, 1998). Yackel and Barber (2000) derived a method to estimate ponds over first-year ice using synthetic aperture radar, and Howell et al. (2005) developed a technique to identify ponds and other ice types from QuikSCAT data. Pond fraction over Baffin Bay sea ice has been estimated from satellite observations by Markus et al. (2003) and over the Beaufort and Chukchi Seas by Tschudi et al. (2001, 2003, 2005). This study was the first to characterize melt pond cover over a large region of the Arctic Ocean for the duration of a melt season.

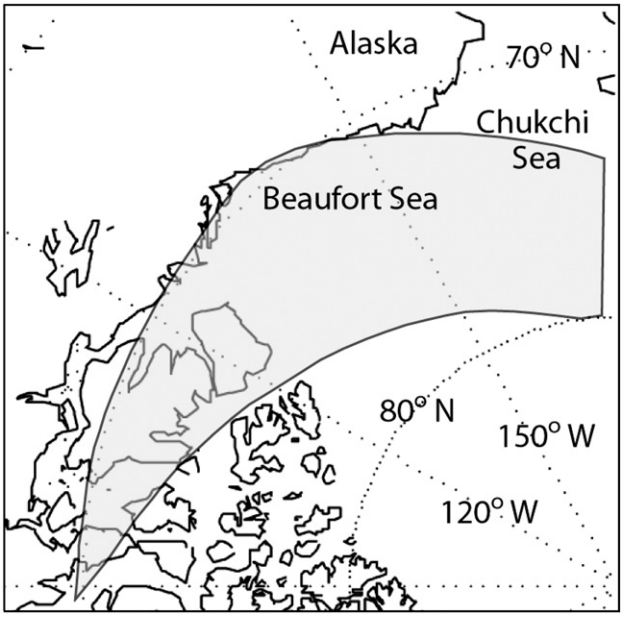

Fig. 1. Melt pond coverage area used in this study. The land areas were omitted.

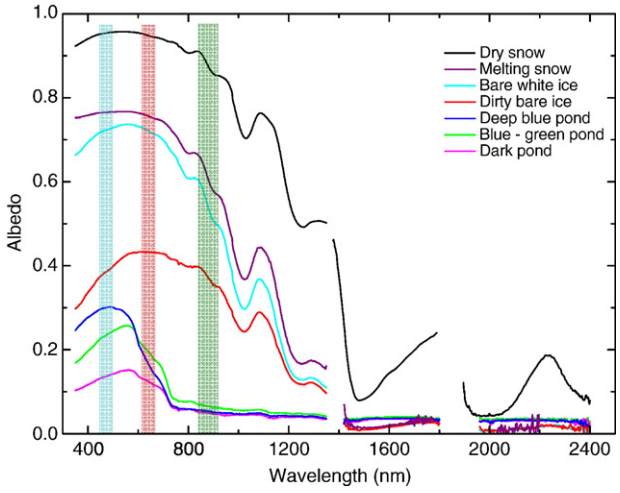

Fig. 2. Spectral reflectance of surface feature types measured near Barrow, Alaska, June 2004. MODIS spectral coverage for, from left to right, bands 3,1,2.

The overall goal of this study was to develop a technique to determine the evolution of melt pond coverage on Arctic sea ice. The method applied MODIS (Moderate Resolution Imaging Spectroradiometer) observations to retrieve melt pond fraction by utilizing the spectral differences between ponds and sea ice. The key feature of this approach was the exploitation of the frequent temporal coverage and comprehensive spectral information available from MODIS to provide pond information at sampling frequencies and over areas sufficiently large to be useful for climate studies and model evaluation. The resulting dataset contained pond fraction covering the majority of the Beaufort Sea and portions of the Chukchi Sea (Fig. 1) spanning the 2004 melt season.

Below, the spectral basis for the approach is first introduced, including a review of in-situ field observations near Barrow, Alaska. Next, the algorithm derivation for MODIS retrievals is described, followed by a validation discussion that makes use of high-resolution aerial photographs obtained using Aerosonde unmanned aerial vehicles (UAVs). This is followed by a discussion of the temporal and spatial variability of MODIS-derived pond fraction for the summer of 2004.

2. In situ spectral measurements

In situ spectral reflectance measurements were instrumental to the technique of deriving pond, ice, and open water fractional coverage from MODIS. To provide these data, on-ice measurements of spectral albedo (Fig. 2) and BRDF (Bidirectional Reflectance Distribution Function) were conducted on the sea ice

Table 1
Spectral reflectance(r_i, unitless) of the ice types used in the pond algorithm over the MODIS channels, acquired June 2004 near Barrow, AK

MODIS channel #	Bandwidth (nm)	Pond r_i	White ice r_i	Snow-covered ice r_i	Open Water r_i
1	620–670	0.16	0.75	0.95	0.08
2	841–876	0.07	0.56	0.87	0.08
3	459–479	0.22	0.76	0.95	0.08

near Barrow, Alaska on June 11–16, 2004 using an Analytical Spectral Devices Fieldspec Pro. This instrument has a spectral range from 350 to 2500 nm, with a response time of less than one second. Ten scans were averaged for each measurement of incident and reflected irradiance. Pairs of incident-reflected measurements were made in about 5 s. Albedo measurements were made using an irradiance collector based on a Spectralon white reference.

The surface albedo measurements were made on the Chukchi Sea side of Point Barrow. The melt season was quite advanced, with significant ponding and bare ice. Observations were performed each day at several sites selected to include the variety of ice conditions present: melting snow, bare deteriorating ice, and melt ponds. The dry snow albedo was measured at the same general location in April 2002. Pond conditions ranged from new shallow ponds to mature ponds tens of centimeters deep. The pond albedos encompassed the range of values observed during time series experiments of longer duration (Grenfell & Perovich, 2004; Perovich et al., 2002a). The albedos measured at the sites were representative of optically thick bare and ponded first year ice.

In addition to the specific site observations, the spatial variability of albedo was investigated by measuring albedo along 100-m-long transect lines. Spectral albedos were measured every 5 m along the lines to examine small scale spatial variability of albedo and to determine estimates of areally averaged albedo. These lines included a temporally evolving mix of bare ice and melt ponds.

Although the spectral reflectance measurements were performed over first-year ice only, the ponds observed were distinctly different types (Fig. 2). Pond reflectances over multiyear ice observed during SHEBA (Perovich et al., 2002a) fell within the range of variability observed on the fast ice near Barrow. In the algorithm to determine pond coverage from MODIS observations, a mean pond reflectance using the recent Barrow observations was implemented to estimate pond fraction over first-year and multiyear ice.

Reflectance of ice and particularly ponds varied within the surface study area. Ponds could not be individually observed with MODIS, so the use of a mean reflectance distribution of observed ice types (including ponds) was the best way to minimize the possible error in the MODIS algorithm. The reflectances we used in our algorithm development were reasonably representative of surface conditions within the Beaufort and Chukchi seas, but we could not quantify that without additional in-situ reflectance measurements spanning the full range of surface conditions. This is an issue with all regional algorithms, in terms of how well they represent other locations.

3. Deriving pond fraction from MODIS data

The technique to estimate melt pond coverage involved solving the following set of linear equations for a_i, the fractional coverage of each surface feature:

$$\left[\sum a_i r_i = R\right]_k, \quad \sum a_i = 1 \tag{1}$$

R is the reflectance for each MODIS pixel for band k (k=1,2,3), and r_i represents the spectral reflectance for each surface feature. In this study, we designated four surface feature types: melt ponds, open water, snow-covered ice, and white ice. The white ice category rose from the observation of bare ice at Barrow that had a white appearance due to the presence of a surface scattering layer. This layer was typically a few centimeters thick and consisted of small fragments of deteriorated ice. This ice type, as well as the other types, appeared to be abundant when examining aerial photographs within the region of interest. Another ice type that could be observed, especially in multiyear floes, is blue ice. However, using the available data, it was impossible to differentiate this ice type from flooded (or shallow ponds on) multiyear ice, as these types had similar spectral signatures. As a result, there are areas of blue ice that were included in the ponded ice classification. However, other than in areas of deformation where blue ice was visible as blocks in ridges or rubble fields, cases where expanses of blue ice are visible were typically limited to situations when frozen ponds are wind-scoured to be free of snow. The error on pond coverage was therefore likely to be small.

The set of linear equations (also shown in (1)) used for this study are:

$$\begin{aligned} a_1 r_{11} + a_2 r_{21} + a_3 r_{31} + a_4 r_{41} &= R_1 \\ a_1 r_{12} + a_2 r_{22} + a_3 r_{32} + a_4 r_{42} &= R_2 \\ a_1 r_{13} + a_2 r_{23} + a_3 r_{33} + a_4 r_{43} &= R_3 \\ a_1 + a_2 + a_3 + a_4 &= 1 \end{aligned} \tag{2}$$

To solve for the fractional coverages (a_i) for each MODIS pixel, we used the MODIS surface reflectance product (MOD09) for R_i. MOD09 was chosen because it utilized several MODIS channels to estimate the reflectance as it would appear at the surface, correcting for atmospheric water vapor and BRDF (Vermote et al., 1997; 2002). MODIS bands 1-3 were used for this analysis (Table 1, Fig. 2); the MOD09 product had a 500 m pixel size. The product was built from one to several overpasses of the EOS Terra satellite, which reduced the effect of cloud cover. However, persistent cloud cover did not allow for a view of the surface (see the end of this section for more details).

The corresponding surface reflectance value for each surface feature (r_i) was observed for the area shown in Fig. 1 using on-ice measurements obtained during June 2004 near Barrow, Alaska, as discussed in the previous section. Table 1 and Fig. 2 depict the spectral reflectance of a few ice types observed during this campaign and the coverage of MODIS bands 1–3, which were utilized for this study. Note that 3 melt pond types were observed and a mean pond spectral reflectance was applied in the pond estimation algorithm. Open water reflectance was

obtained from observations during the SHEBA field experiment (Pegau & Paulson, 2001). Since reflectances were specified from field observations, the coefficients in Eq. (2) were not general to all surface conditions.

The variability in ice type reflectance affected the computed areal coverage of each ice type using Eq. (2). For our observations on the landfast ice off the coast of Barrow, the ice type with the most variability was ponded ice. For one day of observation, we applied a varying range of melt pond reflectances and compared the results to pond coverage observed by the UAV digital cameras (as discussed in the next section), and found that using the mean pond reflectance in Eq. (1) obtained the closest match to the UAV-obtained pond coverage.

The MODIS pond estimation technique was applied to each MOD09 pixel for two data granules (h13v01 and h14v01) for the period June 1–Sept 1, 2004 (92 sets of granules) to produce a daily melt pond coverage (Fig. 3). Data granules are standard areas used to produce MODIS (and other data products) from a series of satellite overpasses. The region formed by these 2 data granules defined the study area for this project. The pond cover was higher near the coast, in areas of land-fast ice, and diminished away from the coast and into the ice pack. Flooded ice at or near the ice-floe edge also contributed to the high estimated fraction of melt ponds, due to its similar spectral signature. Analysis of UAV photos suggested this contribution to be small (<2%), however.

4. Validation

Evaluation of the technique to estimate melt ponds from MODIS reflectance has been performed using high-resolution digital imagery acquired by Aerosonde unmanned aerial vehicle (UAV) flights within the area of interest. The Aerosonde (Fig. 4) is a small (wingspan ~3 m), robotic aircraft designed to undertake a wide range of operations in a highly flexible and relatively inexpensive mode (Curry et al., 2004; Holland et al., 1992; Holland et al., 2001; Maslanik et al., 2002). The aircraft,

Fig. 4. An Aerosonde UAV in a landing approach during one of the Barrow, Alaska-based missions.

developed by a US-Australian consortium, entered limited operations in 1999, with subsequent improvements and upgrades for cold weather operations and general performance improvements. Several successful deployments at Barrow, Alaska have been accomplished by Aerosonde and Aerosonde North America (See www.aerosonde.com for details) from 1999–2006, yielding over 1000 flight hours, acquired primarily during spring and summer flights over the Beaufort and Chukchi seas.

To evaluate the MODIS-derived pond cover estimates, UAV Flights were conducted from June 5 to July 5, 2004 from the Ukpeagvik Inupiat Corporation's Naval Arctic Research Laboratory (UIC-NARL) airfield near Barrow. Four UAVs were flown over the course of this project, including 11 flights (~61 flight hours) dedicated to the mapping of melt pond, ice, and open water fractional coverage. Flight altitudes were typically about 700 m. One flight pattern was designed to fill about 400 MODIS (500 m) pixels by flying adjacent, overlapping flight tracks within a 10×10 km box, aligned to yield approximately 30% overlap between photos from adjacent tracks.

The pond mapping flights deployed a downward-looking Olympus C-3030 digital camera, which acquired visible-wavelength images at intervals that ensured along-track overlapping coverage of the sea ice below. The photo interval was controlled by the aircraft's onboard computer, and could be

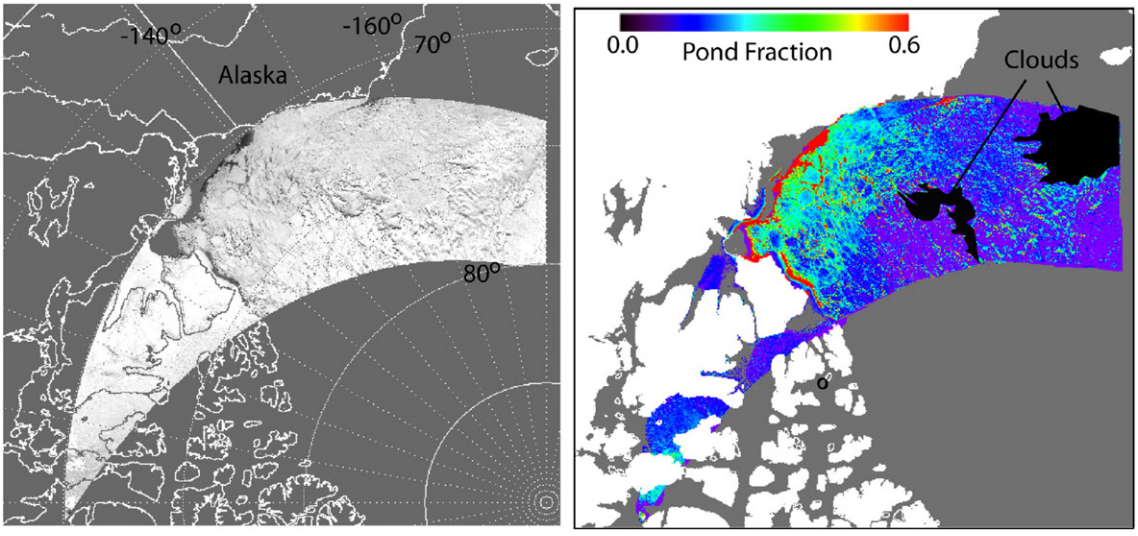

Fig. 3. MODIS Channel 1 reflectance (left) and derived pond coverage (right) for June 13, 2004 in 500 m EASE-grid format. Black polygons are masked areas of cloud cover.

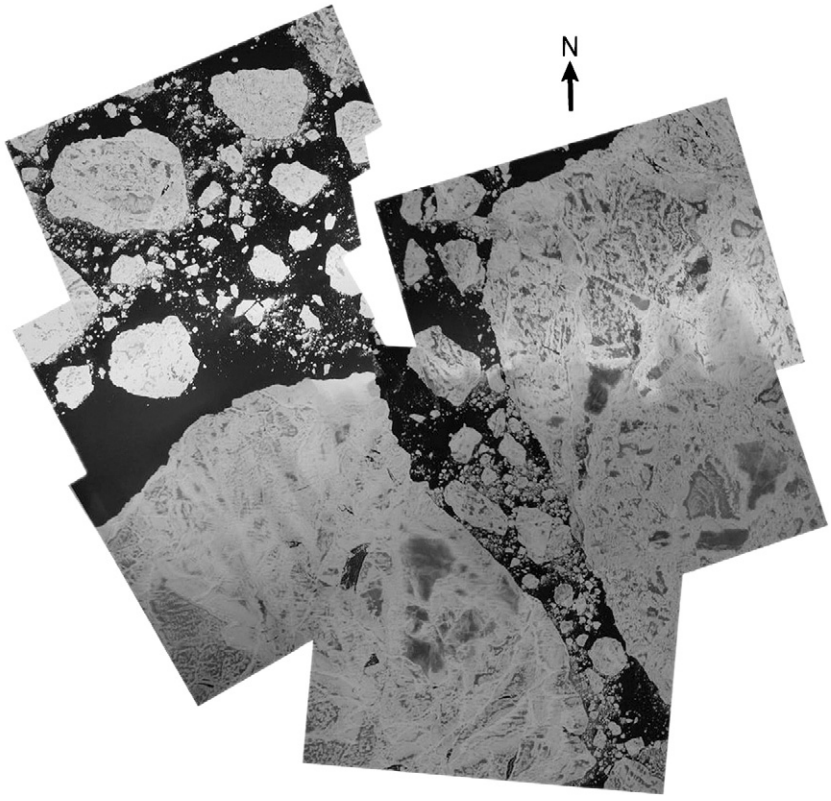

Fig. 5. Mosaic produced by overlapping 7 Aerosonde digital camera images.

varied by the ground controller during flight. Image resolution was typically sub-meter. All color digital images obtained by the nadir-looking camera on the Aerosonde were georeferenced using the GPS position and time information recorded onboard the aircraft. An example of typical ice conditions in the area is shown in the mosaic of UAV photos in Fig. 5.

All digital photographs (e.g. Fig. 6) within a 10 × 10 km box (with continuous coverage) were processed with a computer program written in-house for this study. The classification routine used thresholds applied to the relative brightness of red, blue and green portions of each image pixel to separate melt ponds (and open water) from the ice cover, assuming pure pixels of each surface type. This program allowed for user intervention (i.e. to change the thresholds), which permitted the user to compensate for changes in brightness made by the digital camera's automatic gain control. The effects of camera gain were minimized during image acquisition by using a meter setting that averaged over most of the field of view rather than a center spot, but some variations still needed to be accounted for manually. For this, the user compared the original image to the classified image before proceeding to the next image for processing. This processing was applied to individual photographs rather than to mosaics such as Fig. 5 so that brightness adjustments could be made from image to image. It is estimated based on visual interpretation that this classification technique was accurate to 1–2%. Most error occurs on the edge of the ice or in areas of small, broken ice floes (brash ice), where submerged ice was spectrally similar to ponds. The MODIS classification technique would also misclassify these areas, so it was not expected that this error should contribute to any mismatch between MODIS and UAV pond coverages.

The collection of photos spanning a 10 × 10 km box pattern on June 13, which were acquired under clear skies, were processed to determine the melt pond fraction and compared to the MODIS-derived coverage over the same area (centered at 71.8 N, 156.5 W) (Fig. 7). The UAV and MODIS-derived pond fractions were sorted from lowest to highest, as the geolocation errors in the MODIS pixel (up to 250 m) did not permit a pixel by pixel comparison. Note that these fractions were the percentage of ponds in each UAV pixel (instead of just over ice), allowing for a direct comparison to the MODIS pond estimation technique.

The mean pond fractions found were 14.9% for MODIS and 16.4% for the Aerosonde photos in the 10 × 10 km box, with variances of 1.4% and 0.4%, respectively. The agreement in the mean suggested that the technique to estimate pond fraction using MODIS observations produced a realistic result, permitting this approach to be extended to the entire study area. It is also apparent in this comparison that MODIS tended to overestimate pond fraction in area of high pond coverage and underestimate over low pond coverage. This suggests that the short-term variability in pond coverage was more gradual than the MODIS data predicts. Pond fraction obtained from MODIS and UAV observations were compared for a second case (Fig. 8), and a similar distribution for both techniques were found. Therefore, the agreement and general characteristics of the melt pond estimates are not site-specific.

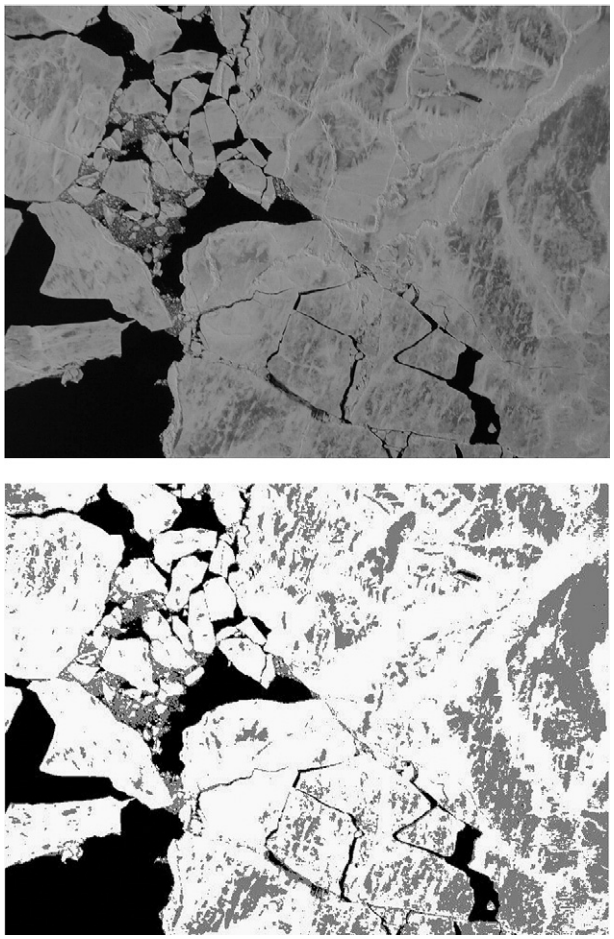

Fig. 6. (Top) Digital camera image acquired during an Aerosonde flight on June 13, 2004. Photo width is about 700 m. (Bottom) Same photo, analyzed to estimate pond fraction (identified ponded areas in grey).

The most likely contributors to the discrepancies in pond coverage estimates between the two approaches included geolocation issues and the representativeness of the in situ reflectance data used. The camera images varied in size as the aircraft altitude changed along the track. The largest geolocation error occured when comparing the nearest MODIS pixel to the Aerosonde picture location. The GPS aircraft position was accurate to within about 15 m, while the MODIS geopositioning accuracy likely introduced location errors of up to 250 m.

Ice motion that occurred between the Aerosonde overflight and the EOS Terra overpass also added to the collocation uncertainty. The MODIS product used in this analysis was a gridded product composed of several overpasses acquired at different times during the same day, so precise geolocation errors would have to be estimated pixel by pixel. However, Fig. 7 considered melt pond percentage over the complete 10 × 10 km box rather than a pixel by pixel comparison. This greatly reduced the contribution of geolocation error, as ice motion during the day would move a small amount of MODIS pixels into or out of the box covered by the Aerosonde photo mosaic. Using daily satellite-derived ice motion data (Emery et al., 1997; Fowler et al., 2003), ice drift velocity was calculated for the comparison

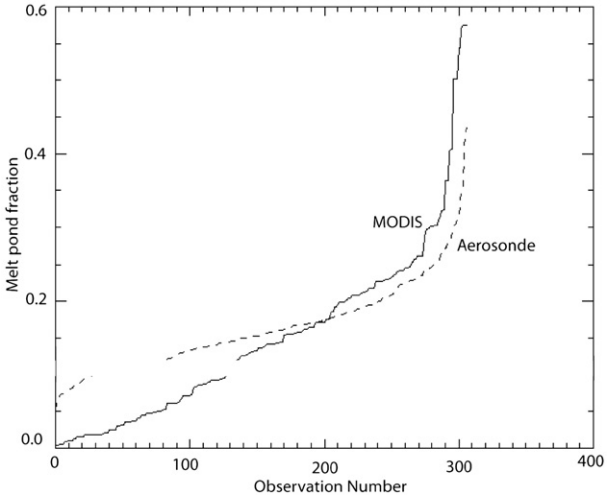

Fig. 7. Aerosonde vs MODIS estimates of pond cover over a 10 × 10 km box on June 13, 2004. Observation # refers to either a MODIS pixel or digital photo from the Aerosonde.

area. Mean ice motion on 13 June 2004 was east to west, at about 1 km/day on average. Given the differences in time between the MODIS and UAV overpasses, the likely displacement of the ice pack therefore was 1 km or less on 13 June.

The analysis here used spectral reflectance of ponds observed near the coast of Barrow, and although the observations were made during the same time period as the Aerosonde flights, the pond (and other ice type) reflectance can vary significantly within the study region. Evidence of pond reflectance variability was observed in the study area by examining relative reflectances for different ponding conditions. Even within small regions, pond and ice spectral reflectance can exhibit high variability (Barber & Yackel, 1999; Hanesiak et al., 2001; Yackel et al., 2000). Factors such as ice thickness, ice type (first-year or multiyear), snow wetness and contaminants within the ice can affect spectral reflectance, so both temporal and spatial variations are likely. However, as Fig. 9 suggests, a

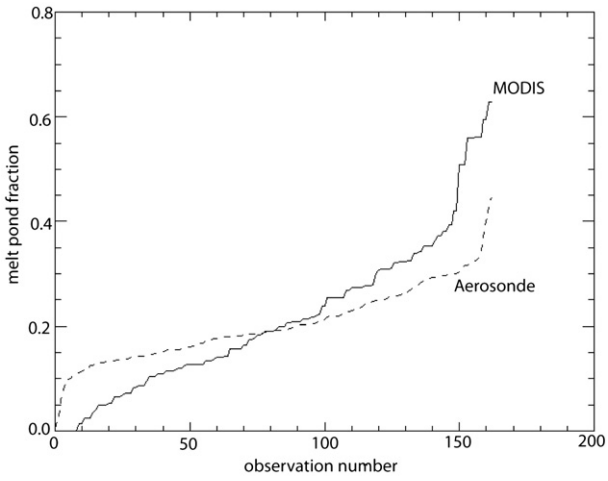

Fig. 8. MODIS vs Aerosonde melt pond fraction on June 12, 2004. Analysis area was approximately 6 × 6 km, over multiyear ice centered near 78 °N, 157 °W.

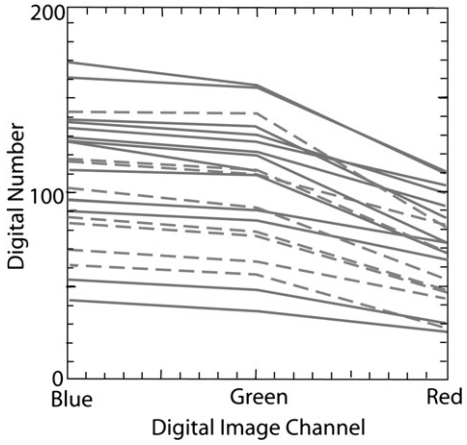

Fig. 9. Pond reflectance obtained from analysis of Aerosonde digital camera images obtained near Barrow during June/July 2004. Solid lines are early-season (June) ponds. Dashed lines are mid-season (July) ponds.

typical characteristic of ponds was the decrease in the reflectance in the red part of the spectrum as ponds mature, which was also apparent in the in situ data shown previously in Fig. 2. Our application of the mean spectral reflectance for ponds, along with the particular reflectances observed off the coast of Barrow, has resulted in mean melt pond coverage that is closest to the UAV observations. The 1.5% difference between the 2 methods (14.9% for MODIS, 16.4% for Aerosonde) in the region compared in Fig. 7 grows to about 10% when the largest spectral reflectance values (deep blue pond) were implemented (MODIS pond coverage is overestimated), while MODIS greatly underestimates (by roughly the same percentage) the pond fraction when the smallest reflectance values (dark pond) were used. A more sophisticated approach, suggested for future applications, would be to vary the pond spectral signature to "mature," as is suggested by data in Fig. 9. This variation would be applied temporally (through the melt season) as well as spatially (as the melt season progresses north).

5. Analysis of pond temporal and spatial variability

Given this assessment of the MODIS algorithm performance, we investigated the evolution of pond cover on the ice through the summer 2004 melt season for the area of interest (Fig. 10). The indicated melt pond coverage was corrected to show the coverage on the ice only. The algorithm obtained the fraction of ponds represented in each MODIS pixel, but each pixel may have contained ice and open water. In Fig. 10, the open water (broken line) was removed, resulting in pond coverage over sea ice only. Note that ponds that have melted through the ice were also classified as open water, since they were holes in the ice and were the same spectrally (and in composition) as open water. In fact, it can be argued that since such ponds are equivalent to leads in terms of water and heat exchange, treatment of these areas as open water in the algorithm was physically valid. A similar argument can be made for dark, shallow ponds on thin, heavily-melted first-year ice, or for areas where first-year ice is flooded. A melt pond distribution through the summer 2004 melt season in our area of study is approximated by the dashed line, and is represented by:

$$\mathrm{mp}(d) = a_0 + a_1 d + a_2 d^2 + a_3 d^3; \quad (3)$$

where d is the day number (which ranges from 153 to 243), mp the melt pond fraction and a the coefficients for this cubic polynomial fit: $a(0) = -8.364$, $a(1) = 0.1160$, $a(2) = -5.034 * 10^{-4}$, $a(3) = 7.103 * 10^{-7}$. Eq. (3) represents the melt pond distribution through summer 2004 in the study region only. It is not necessarily a general relationship outside of the study area or for other melt seasons.

The pond fraction was found to increase rapidly early in the melt season, climbing from 10% on June 1 to about 40% by the 1st of July. During this period, warm air temperatures (exceeding 50 °F) were observed near Barrow, which likely contributed to the subsequent rapid melt of the sea ice. Furthermore, peak solar insolation (on June 21) and an abundance of clear skies led to more available solar radiation to be absorbed by the ice pack, enhancing melt. Rapid pond development early in the melt season was also observed during the SHEBA campaign (Perovich et al., 2002b; Tschudi et al., 2001).

After early July, pond coverage was variable both spatially and temporally. The large variability was typical of rapid temporal and spatial changes observed in other analyses (e.g., Eicken et al., 2004). The decline in pond fraction beginning near the end of July (day 208 in Fig. 10) and again in mid-August (day 230) was likely due to drainage of ponds, consistent with other studies that have observed similar transitions (e.g. Drinkwater & Carsey, 1991; Eicken et al., 2004; Fetterer & Untersteiner, 1998). Some of the variability later in August may have resulted from freeze and thaw events in the northern portion of the data coverage. Part of the variability can also be explained by portions of the ice appearing and disappearing due to clouds (see cloud discussion at end of this section). Ice was moving through

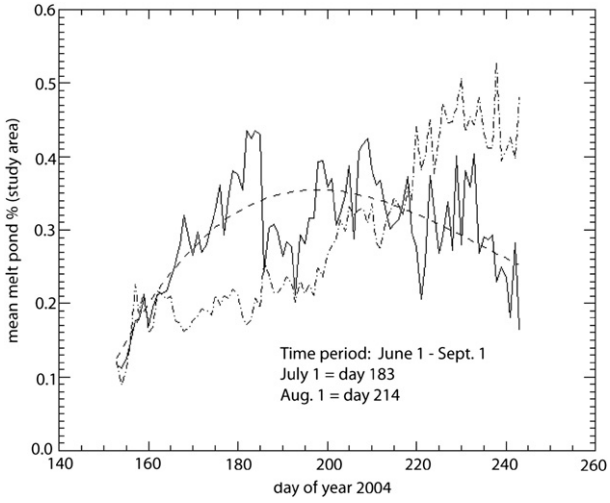

Fig. 10. Evolution of pond fraction (solid line) through the summer melt season in this study's area of interest. Pond fraction has been corrected for open water (i.e. this is pond fraction on the ice). Open water is shown as broken line, smoothed melt pond distribution as dashed line.

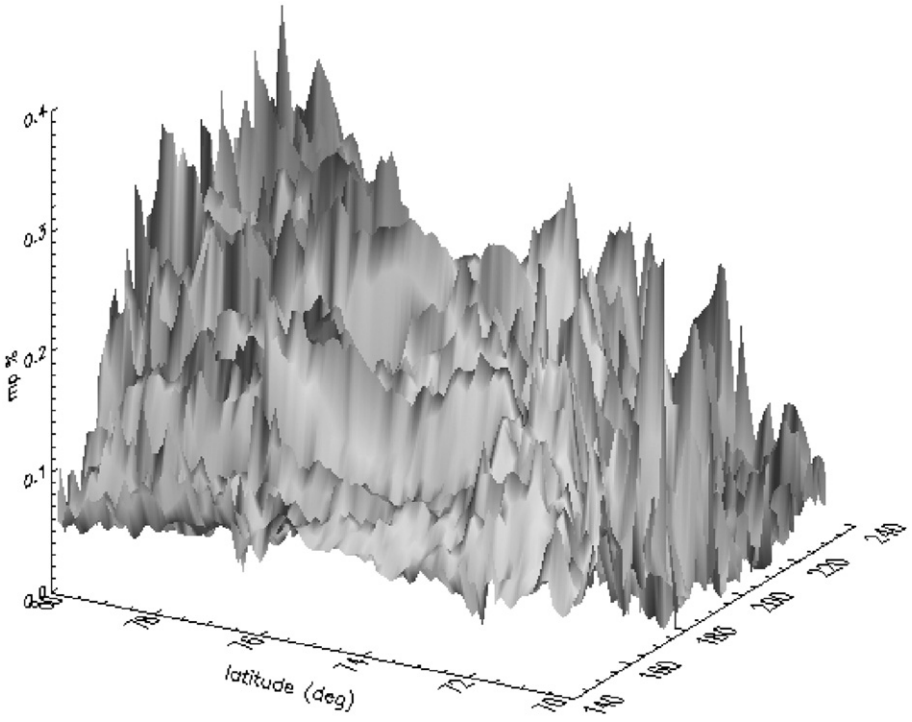

Fig. 11. Latitudinal and temporal variation of pond cover on sea ice (i.e. corrected for open water, as in previous figure) over the study area. The unmarked axis is day #.

the area of interest at a rate of about 1 km/day. In general, a westerly ice motion occurs in this area, with ice moving in from the eastern Beaufort Sea.

Pond coverage returned to near the June 1 value by the end of the melt season. Pond fraction decrease could in part be attributed to ponds that melted through the ice, as these ponds were then classified as open water, since they were essentially holes in the ice exposing the underlying ocean. The increase in open water fraction during this period was evidence of this phenomenon. The gradual decline in pond fraction may also be a result of a cooling of air temperatures, which led to freezing of the pond surface, allowing some ponds to be covered by intermittent snowfall and not detected. Drainage of ponds also contributed to pond coverage decline as the melt season progressed.

The variation of pond cover on the ice through the melt season by latitude is shown in Fig. 11. It appears that the mean seasonal pond fraction was greater in higher latitudes, due in part to the larger ice concentration in that region, which, along with thicker ice, allows for less runoff and thus more water was retained to form ponds. The progression of pond fraction was delayed in higher latitudes, most likely due to the general warming from south to north. More active ice kinematics in the intermediate latitude range, and perhaps thinner ice in this region, may also have contributed to increased pond drainage. Note that the maximum pond fraction was later at 80°N than 70°N, and later than the mean distribution.

Retrieval of pond coverage in the region of interest was restricted by the presence of clouds, which obscured the view of the surface by MODIS. The daily MODIS reflectance product (MOD09) was constructed from numerous overpasses by the EOS TERRA and AQUA satellites, which reduced the effect of cloud cover. Portions of the study region were viewed by each satellite about 12 times per day. MOD09 was built from one or more clear-sky pixels from each view, and could therefore maximize the clear sky present in the daily gridded product. Although persistent (throughout one day) cloudiness did not allow for pond estimation, the use of multiple MODIS overpasses resulted in a marked improvement over previous cloud cover observations in this region, which can range from 63 to 97% (Intrieri et al., 2002). In general, daily persistent cloud cover grew more prevalent as the melt season advanced (Fig. 12), but at least half of the study area was observable for most (82%) of the days analyzed.

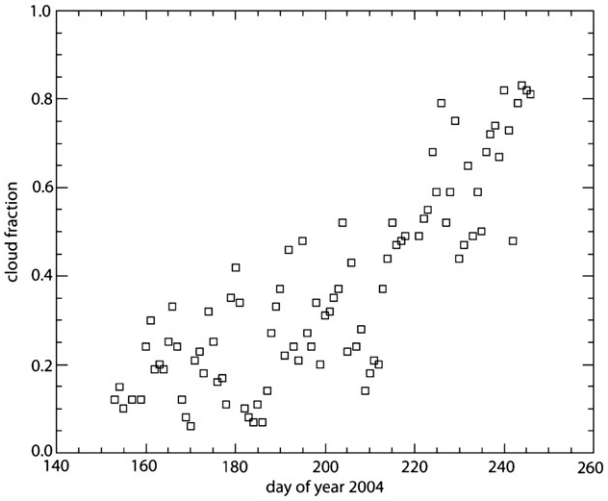

Fig. 12. Persistent daily cloud coverage in the study region. Pond coverage cannot be estimated from satellite under cloudy skies.

6. Summary

The coverage of melt ponds on sea ice greatly influences the amount of solar energy absorbed by the ice pack, and is thus an important parameter for estimating the rate of summer sea ice melt, which has been shown to be an important issue in climate change. A mixed-pixel algorithm to estimate the summer evolution of pond coverage over the Beaufort and Chukchi Seas has been developed. The technique utilized the daily MODIS surface reflectance product (MOD09) over sea ice and open water in the region of interest to estimate the coverage of melt ponds. UAV digital camera images of pond coverage confirmed that this technique accurately estimated pond coverage in the given region, and can thus be extended to the rest of the Arctic ice cover for this and other melt seasons.

The coverage of ponds in the study area increased rapidly during early spring, followed by a gradual decline to pre-melt coverage in early autumn. This general trend was also observed during SHEBA, when an early season rainfall resulted in a quick formation of numerous melt ponds.

The MODIS and Aerosonde-derived pond coverage datasets should be useful to the remote sensing and modeling community. To date, melt pond fraction has only been observed on local (field studies) and intermediate (airborne) scales, and typically not for a full melt cycle. The result of this research is the first large-scale characterization of pond coverage through the melt season. Mapping of the spatial coverage and temporal evolution of pond fraction has a variety of potential applications, including improvement of the treatment of albedo within models, serving as a climatic change signal through documentation of the inter-annual variability in melt processes, and quantifying the error introduced by ponds in ice concentrations derived from passive microwave imagery. Melt pond fraction is a key parameter in estimating the large-scale evolution of albedo and the overall surface energy budget of the ice cover. Melt pond coverage may also prove to be related to ice morphology and ice type, which would provide additional information to characterize spatial and interannual variability in the ice cover.

The daily melt pond coverage for summer 2004 in the region of study will be available at the National Snow and Ice Data Center (NSIDC). In addition to melt pond fraction, estimates of the coverage of white ice, snow-covered ice, and open water will be included, as well as clear-sky reflectances for MODIS channels 1–4.

Acknowledgments

We extend thanks to 3 anonymous reviewers, whose suggestions greatly improved the quality of this paper. This study was funded by NASA grants NNH04AA68I and NAG5-12399.

References

Anderson, M. R., & Drobot, S. D. (2001). Spatial and temporal variability in snowmelt onset over Arctic sea ice. *Annals of Glaciology*, *33*, 74−78.

Barber, D. G., & Yackel, J. J. (1999). The physical, radiative and microwave scattering characteristics of melt ponds on Arctic landfast sea ice. *International Journal of Remote Sensing*, *20*(10), 2069−2090.

Cavalieri, D., Gloersen, P., & Campbell, W. J. (1984). Determination of sea ice parameters with the Nimbus 7 SMMR. *Journal of Geophysical Research*, *89*(D4), 5355−5369.

Comiso, J. C. (2002). A rapidly declining perennial sea ice cover in the Arctic. *Geophysical Research Letters*, *29*(20), 1956. doi:10.1029/2002GL015650

Curry, J. A., Maslanik, J. A., Holland, G., Pinto, J., Tyrrell, G., & Inoue, J. (2004). Applications of Aerosondes in the Arctic. *Bulletin of the American Meteorological Society*, *85*, 1855−1861.

Curry, J. A., Schramm, J. L., & Ebert, E. E. (1995). Sea-ice albedo climate feedback mechanism. *Journal of Climate*, *8*(2), 240−247.

Drinkwater, M. R., & Carsey, F. (1991). Observations of the late-summer to fall sea ice transition with the 14.6 GHz SEASAT Scatterometer. *Proceedings of the International Geoscience And Remote Sensing Symposium, held in Helsinki, Finland, IEEE Publications* (pp. 1597−1600).

Eicken, H., Grenfell, T. C., Perovich, D. K., Richter-Menge, J. A., & Frey, K. (2004). Hydraulic controls of summer Arctic pack ice albedo. *Journal of Geophysical Research*, *109*, C08007. doi:10.1029/2003JC001989 12 pgs.

Eicken, H., Martin, T., & Reimnitz, E. (1994). Sea ice conditions along the cruise track. In D. K. Futterer (Ed.), *The Expedition Arctic '93. Leg ARK-IV/4 of RV Polarstern 1993Ber. Polarforsch*, *Vol. 149*. (pp. 42−47).

El Naggar, S., Garrity, C., & Ramseier, R. O. (1998). The modeling of sea ice melt-water ponds for the High Arctic using an airborne line scan camera, and applied to Satellite Special Sensor Microwave/Imager (SSM/I). *International Journal of Remote Sensing*, *19*, 2373−2394.

Emery, W. J., Fowler, C. W., & Maslanik, J. A. (1997). Satellite derived Arctic and Antarctic sea ice motions: 1988–1994. *Geophysical Research Letters*, *24*(8), 897−900.

Fetterer, F., & Untersteiner, N. (1998). Observations of melt ponds on Arctic sea ice. *Journal of Geophysical Research*, *103*, 24821−24835.

Fowler, C., Emery, W., & Maslanik, J. A. (2003). Satellite derived arctic sea ice evolution Oct. 1978 to March 2003. *Transactions on Geoscience and Remote Sensing Letters*, *1*(2), 71−74.

Grenfell, T. C., & Perovich, D. K. (2004). The seasonal evolution of albedo in a snow-ice-land-ocean environment. *Journal of Geophysical Research*, *109*(C1), C01001. doi:10.1029/2003JC001866

Hanesiak, J. M., Barber, D. G., De Abreu, R. A., & Yackel, J. J. (2001). Local and regional albedo observations of arctic first-year sea ice during melt ponding. *Journal of Geophysical Research*, *106*(C1), 1005−1016.

Holland, G. J., McGeer, T., & Youngren, H. (1992). Autonomous Aerosondes for economical atmospheric soundings anywhere on the globe. *Bulletin of the American Meteorological Society*, *73*, 1987−1998.

Holland, G. J., Webster, P. J., Curry, J. A., Tyrell, G., Gauntlett, D., Brett, G., et al. (2001). The Aerosonde robotic aircraft: a new paradigm for environmental observations. *Bulletin of the American Meteorological Society*, *82*(5), 889−901.

Howell, S. E. L., Yackel, J. J., De Abreu, R., Goldsetzer, T., & Breneman, C. (2005). On the utility of SeaWinds/QuikSCAT data for the estimation of the thermodynamic state of first-year sea ice. *IEEE Transactions on Geoscience and Remote Sensing*, *43*(6), 1338−1350.

Intrieri, J. M., Shupe, M. D., Uttal, T., & McCarty, B. J. (2002). An annual cycle of Arctic cloud characteristics observed by radar and lidar at SHEBA. *Journal of Geophysical Research*, *107*(C10), 8030.

Markus, T., Cavalieri, D. J., Tschudi, M. A., & Ivanoff, A. (2003). Comparison of aerial video and Landsat 7 data over ponded sea ice. *Remote Sensing of Environment*, *86*, 458−469.

Maslanik, J. A., Curry, J., Drobot, S., & Holland, G. (2002). Observations of sea ice using a low-cost unpiloted aerial vehicle, Proc. 16th. *IAHR International Symposium on Sea IceInt. Assoc. of Hydraulic Engineering and Research*, *Vol. 3* (pp. 283–287).

Maslasnik, J. A., Fowler, C., Stroeve, J., Drobot, S., & Zwally, J. (2007). A younger, thinner Arctic ice cover: increased potential for rapid, extensive ice loss. *Geophysical Research Letters*, *34*, L24501. doi:10.1029/2007GL032043.

Maykut, G. A., Grenfell, T. C., & Weeks, W. F. (1992). On estimating the spatial and temporal variations in the properties of sea ice in the polar oceans. *Journal of Marine Systems*, *3*, 41−72.

Pegau, W. S., & Paulson, C. A. (2001). The albedo of Arctic leads in summer. *Annals of Glaciology*, *33*, 221−224.

Perovich, D. K., Grenfell, T. C., Light, B., & Hobbs, P. V. (2002). Seasonal evolution of the albedo of multiyear Arctic sea ice. *Journal of Geophysical Research*, *107*(C10), 8044. doi:10.1029/2000JC000438

Perovich, D. K., Tucker, W. B., III, & Ligett, K. A. (2002). Aerial observations of the evolution of ice surface conditions during summer. *Journal of Geophysical Research*, *107*(C10), 8048. doi:10.1029/2000JC000449

Perovich, D. K., & Tucker, W. B., III (1997). Arctic sea ice conditions and the distribution of solar radiation during summer. *Annals of Glaciology*, *25*, 445−450.

Rothrock, D. A., Zhang, J., & Yu, Y. (2003). The Arctic ice thickness anomaly of the 1990s: a consistent view from models and observations. *Journal of Geophysical Research*, *108*(C3), 3083. doi:10.1029/2001JC001208

Serreze, M. C., Maslanik, J. A., Scambos, T. A., Fetterer, F., Stroeve, J., Knowles, K., et al. (2003). A record minimum arctic sea ice extent and area in 2002. *Geophysical Research Letters*, *30*(3), 1110.

Stroeve, J. C., Serreze, M. C., Drobot, S., Gearheard, S., Maslanik, J., Meier, W., et al. (2008). Arctic sea ice in 2007. *EOS*, *89*(2), 13−14.

Tschudi, M., Curry, J. A., & Maslanik, J. A. (2001). Airborne observations of summertime surface features and their effect on surface albedo during SHEBA. *Journal of Geophysical Research*, *D14*(106), 15335−15344.

Tschudi, M. A., Maslanik, J. A., & Curry, J. A. (1997). Determination of areal surface-feature coverage in the Beaufort Sea using aircraft video data. *Annals of Glaciology*, *25*, 434−438.

Tschudi, M. A., Maslanik, J. A., & Perovich, D. K. (2003). Beaufort Sea ice melt pond coverage from MODIS observations. *Proceedings, Amer. Met. Soc. Seventh Conf. on Polar Met. and Ocean., Hyannis, MA*.

Tschudi, M. A., Maslanik, J. A., & Perovich, D. K. (2005). Melt pond coverage on Arctic sea ice from MODIS. *Proceedings, Amer. Met. Soc. Eighth Conf. on Polar Met. and Ocean., San Diego, CA*.

Tucker, W. B., III, Gow, A. J., Meese, D. A., & Bosworth, H. W. (1999). Physical characteristics of summer sea ice across the Arctic Ocean. *Journal of Geophysical Research*, *104*, 1489−1504.

Vermote, E. F., El Saleous, N., & Justice, C. (2002). Atmospheric correction of the MODIS data in the visible to middle infrared: first results. *Remote Sensing of Environment*, *83*(1–2), 97−111.

Vermote, E. F., El Saleous, N. Z., Justice, C. O., Kaufman, Y. J., Privette, J., Remer, L., et al. (1997). Atmospheric correction of visible to middle infrared EOS-MODIS data over land surface, background, operational algorithm and validation. *Journal of Geophysical Research*, *102*(D14), 17,131−17,141.

Yackel, J. J., & Barber, D. G. (2000). Melt ponds on sea ice in the Canadian Archipelago, 2: on the use of RADARSAT-1 synthetic aperture radar for geophysical inversion. *Journal of Geophysical Research*, *105*(C9), 22,061−22,069.

Yackel, J. J., Barber, D. G., & Hanesiak, J. M. (2000). Melt Ponds on Sea Ice in the Canadian Arctic Archipelago: Part 1. Variability in morphological and radiative properties. *Journal of Geophysical Research*, *105*(C9), 22049−22060.